Sonothrombolysis with magnetically targeted microbubbles

Marie de Saint Victor[1], Lester C. Barnsley[1i], Dario Carugo[1ii], Joshua Owen[1], Constantin C. Coussios[1], Eleanor Stride[1*]

[1]Institute of Biomedical Engineering, Department of Engineering Science, University of Oxford, Oxford OX3 7DQ, United Kingdom

i. Present address: Jülich Centre for Neutron Science (JCNS) at Heinz Maier-Leibnitz Zentrum (MLZ), Forschungszentrum Jülich GmbH, Lichtenbergstrasse 1, D-85748 Garching, Germany

ii. Present address: Faculty of Engineering and the Environment, Institute for Life Sciences (IfLS) University of Southampton, Highfield, Southampton SO17 1BJ, United Kingdom

Type of Manuscript: Original Contribution

Submitted to: Ultrasound in Medicine and Biology

No. of Figures: 8

[*] **Correspondence to:** Eleanor Stride

Address: Institute of Biomedical Engineering, University of Oxford, Old Road Campus Research Building, Oxford OX3 7DQ, UK

Telephone: +44(0)1865617747

E-mail: eleanor.stride@eng.ox.ac.uk

Abstract

Microbubble-enhanced sonothrombolysis is a promising approach to increase the safety and efficacy of current pharmacological treatments for ischemic stroke. Maintaining therapeutic concentrations of microbubbles and drugs at the clot site however poses a challenge. The objective of this study was to investigate the efficacy of magnetic microbubble targeting upon clot lysis rates *in vitro*. Retracted whole porcine blood clots were placed in a flow phantom of a partially occluded middle cerebral artery. The clots were treated with a combination of tissue plasminogen activator (0.75μg/mL), magnetic microbubbles (~10^7 microbubbles/mL), and ultrasound (0.5MHz, 630kPa peak rarefactional pressure, 0.2Hz pulse repetition frequency, 2% duty cycle). Magnetic targeting was achieved using a single permanent magnet element (0.08-0.38T and 12-140T/m in the region of the clot). The change in clot diameter was measured optically over the course of the experiment. Magnetic targeting produced a three-fold average increase in lysis rates and linear correlation was observed between lysis rate and total energy of acoustic emissions.

Keywords: magnetic targeting; microbubbles; thrombolysis; ultrasound; clot; passive cavitation detection; drug delivery.

Introduction

Despite recent therapeutic advances, ischemic stroke remains a leading cause of disability and mortality worldwide (Naghavi, et al. 2015, Feigin, et al. 2017). At present, intravenous tissue-plasminogen activator (tPA) is the only thrombolytic drug recommended by the British National Institute of Health and Care Excellence (NICE)(NICE 2008) and the U.S. Food and Drug Administration (FDA) (FDA 1996). It carries however the risk of potentially fatal side effects including intracranial haemorrhage. As a result, intravenous tPA administration is subject to rigid exclusion criteria (American College of Emergency Physicians and American Academy of Neurology 2013). Among the most limiting of these is the therapeutic time frame for intravenous administration of the drug (Barber, et al. 2001). In a study conducted with the California Acute Stroke Pilot Registry, only 4.3% of all ischaemic stroke patients arrived in the Emergency Department within the recommended 3-hour window after stroke onset and were thus eligible for tPA. Of equal concern is the fact that even if all patients had arrived within the required time frame, only 28.6% of them would have been eligible for thrombolytic treatment (California Acute Stroke Pilot Registry Investigators 2005).

Against this background, there is a clear need for an adjuvant therapy that improves the safety and efficacy of thrombolytic treatment. Sonothrombolysis, i.e. the use of ultrasound (US) for enhanced thrombolysis is a minimally or non-invasive physical approach that can be used to enhance the action of tPA, thereby reducing the required dose, or facilitating clot breakdown in the absence of a drug. Multiple *in vitro* and *in vivo* studies have shown that intravenously administered microbubbles can significantly improve the rate of clot breakdown, with or without concomitant use of a thrombolytic drug (Lu, et al. 2016,

Schleicher, et al. 2016). Several clinical trials have also demonstrated accelerated recanalisation of occluded vessels (Molina, et al. 2006, Perren, et al. 2008). The echogenicity of microbubbles may also improve patient safety by enabling continuous treatment monitoring (Xie, et al. 2009).

Further work is however necessary to improve the safety and efficacy of sonothrombolysis protocols. In particular, the hydrodynamic conditions in occluded vessels represent a major challenge since they severely limit the number of microbubbles that can be delivered to and retained at the site of a thrombus (de Saint Victor, et al. 2017). Conjugation of antibodies to the microbubble surface has been investigated as a means of increasing the proximity between microbubbles and the thrombus surface, thereby enhancing their lytic effect (Hagisawa, et al. 2013, Hua, et al. 2014). This approach, however, does not address the challenge of delivering a sufficient concentration of microbubbles to the clot initially. The objective of the present study was therefore to investigate whether magnetic targeting could be used to improve both the delivery and retention of microbubbles to an *in vitro* clot model and whether this could enhance enzymatic sonothrombolysis. In addition, the feasibility of non-invasive acoustic methods for treatment monitoring was evaluated.

Materials and Methods

Clot model

Clots were prepared using whole blood obtained from the carotid artery of a female large white X landrace breed pig. Fresh plasma was employed as the flow medium and prepared by collecting whole blood from the aortic artery of a female large white X landrace breed pig

into citrated blood bags (CPDA-1, Fenwal Inc., Lake Zurich, IL, USA) and spinning the sample at 4,400 revolutions per minute (rpm) in a 15 cm radius centrifuge for 20 min at room temperature to separate blood components. The plasma was stored at -80°C until use. It was defrosted at 37°C for at least 15 min prior to the experiments. All animal work was approved by an animal care and ethics review committee and conformed to the UK Animals (Scientific Procedures) Act 1986.

Clots were formed around silk sutures following a protocol similar to that described by (Meunier, et al. 2007). Briefly, 4-0 size braided silk sutures (Ethicon US LLC, Somerville, NJ, USA) were threaded through 3.4 mm inner diameter, 60 mm long borosilicate cylinders (Aimer Products Ltd, Enfield, UK). Each cylinder was placed in an additive-free 13 mm inner diameter Vacutainer tube (BD, Franklin Lakes, NJ, USA). 2 mL blood samples were then aliquoted into the Vacutainers and incubated for 6 hours in a water bath at 37°C, then at 4°C for 24 hours to allow retraction. The clots were typically of cylindrical shape, with a diameter of 1.7 ± 0.5 mm and a length of approximately 30 mm. They were stored for at least 48h before use, and kept for up to 15 days in degassed phosphate-buffered saline at 4°C. (Holland, et al. 2008) have shown in a similar clot model that, in this timeframe, clot age has no effect on response to tPA.

Flow loop

The experiments were carried out in a 50 x 80 x 55 cm Lucite tank containing approximately 120 litres of filtered, deionised and degassed water which was maintained at 37±1.5°C by a heating circulator (GD100, Grant Instruments, Cambridge, UK). The clots were placed in a flow chamber consisting of an optically and acoustically transparent polyolefin tube (3.2 mm

inner diameter and 0.18 mm wall thickness, Heatshrink-Online Ltd, Huntingdon, UK). The internal diameter of the tube was selected to correspond to the typical dimensions of the middle cerebral artery (Serrador, et al. 2000), one of the cerebral vessels most commonly affected by ischaemic stroke (Demchuk, et al. 2001). A solution of dilute plasma (1.25% v/v fresh frozen plasma in PBS) was circulated once through the chamber at a rate of 3 mL/min by a peristaltic pump (Minipuls 2, Gilson Inc., Middleton, WI, USA). The flow rate was selected to obtain a mean blood velocity past the clot at the lower end of the range observed in a partially occluded middle cerebral artery (Ogata, et al. 2004). Lipid-shelled magnetic microbubbles were infused continuously, along with tPA, into the diluted plasma at a rate of 140 µL/min using a syringe pump (World Precision Instruments Ltd, Hitchin, UK). The final concentrations of tPA and microbubbles in the diluted plasma were 0.75 µg/mL and 8.1 $x10^6 \pm 1.2 \times 10^5$ microbubbles/mL respectively. Four experimental groups were defined: exposure to tPA only, US + tPA, US + tPA + microbubbles (no external magnet), and US + tPA + microbubbles + external magnet.

Magnetic microbubble preparation

Phosphate-buffered saline (PBS) was sourced from Sigma Aldrich (Sigma Aldrich Corporation, St Louis, MO, USA). Tissue plasminogen activator (Actilyse, Boehringer Ingelheim Pharma GmbH & Co. KG, Ingelheim am Rhein, Germany) was reconstituted in water to the concentration of 1 mg/mL and stored in 400 µL aliquots at -80°C. Under these storage conditions, the enzyme is stable for up to a year (Alkatheri 2013, Jaffe, et al. 1989). The phospholipid 1,2 distearoyl-sn-glycero-3-phosphocholine (DSPC) was purchased from Avanti Polar Lipids Inc., Alabaster, USA. The ferrofluid (10 nm spherical magnetite

nanoparticles in isoparaffin, 10% volume fraction) was obtained from Liquids Research Ltd, Bangor, UK.

The protocol for magnetic microbubble preparation was based on the method first described by (Stride, et al. 2009). The microbubbles were prepared by sonication using a 22.5 kHz ultrasonic cell disruptor (Microson XL, Misonix Inc., Farmingdale, NY, USA) operating at level 4, corresponding to an output power of 8 WRMS. Briefly, 15 ml of deionised water were added to 15 mg of DSPC. The sonicating probe was first inserted into this solution for 90 s to disperse the lipid; then it was placed at the air-liquid interface for 15 s to entrain air. Subsequently, 15 µl of the ferrofluid were added to the solution. The microbubble solution was then sonicated again for 30 s with the probe tip fully inserted into the fluid, and for 15 s with the probe tip at the air-liquid interface. The vial was manually shaken vigorously for 45 s. Microbubble concentration and size were assessed as previously described by (Sennoga, et al. 2010). A 10 µl sample was placed on a microscope slide and 25 images were taken with a x40 objective. The images were then analysed using purpose written software in MATLAB (The MathWorks Inc., Natick, MA, USA) to count particles of diameters ranging from 0.2 µm (~ 2 pixels) to 15 µm.

Magnetic targeting

The magnetic field was applied as illustrated in Figure 1, using a single 12.7 mm cubic permanent magnet element (N52 grade NdFeB, NeoTexx, Berlin, Germany). It was placed below the clot at an angle of 45^{o}, its upper vertex in contact with the flow channel directly below the ultrasound focus. During experiments that did not involve magnetic targeting, the magnet was replaced by a stainless steel block of identical dimensions in order to maintain a comparable sound field.

The magnetic field and the magnetic field gradient in the flow chamber were first computed using a numerical model developed by (Barnsley, et al. 2015). The magnetisation value of the magnet, an essential input parameter to the model, was then determined experimentally by measuring the field profile of a single NdFeB element using a three-axis Hall probe connected to a Model 460 3-channel gaussmeter (Lake Shore Cryotronics, Inc.,OH, USA). The field profile was fitted to an analytical expression for the field generated by a cuboid (Engel-Herbert and Hesjedal 2005), yielding a magnetisation value of 1.087×10^{6} $A.m^{-1}$.

Prior to the sonothrombolysis experiment, magnetic targeting efficiency was evaluated. In these experiments, the clot was replaced by a light-coloured phantom of the same dimensions so as to facilitate visualisation of the dark brown microbubble solution. A 1 mL bolus was injected into the flow and images were acquired at 30 frames/s with a digital camera (Canon EOS 500D, Canon Ltd., Reigate, UK). The images were processed with purpose-written code in Matlab (The MathWorks Inc., Natick, MA, USA) to quantify retention of magnetic material over 12 s. In each frame, the region of interest (ROI) was defined as a 3-mm wide window around the axis of the ultrasound transducer. NR(t), the "normalised retention" at a given time point *t*, was defined as

$$\mathrm{NR}(t) = \frac{I(t) - I(t_0)}{I(t_1) - I(t_0)} \qquad (1)$$

where $I(t)$ is the total greyscale intensity in the ROI at time t, t_0 is baseline time (before bolus injection), and t_1 corresponds to bolus arrival in the ROI.

Ultrasound exposure and monitoring

For the ultrasound experiments, two ultrasound transducers were mounted coaxially, as described by (Hockham, et al. 2010). The ultrasound source was a focused, circular, single element, 0.5 MHz transducer (Sonic Concepts, Bothell, WA, USA). The transducer centre frequency was chosen to balance considerations of treatment safety and efficacy. Lower frequency ultrasound is more effective at breaking down blood clots (Nedelmann, et al. 2005) (Schafer, et al. 2005) and is less attenuated by tissue and bone, but safety concerns have been raised in several studies conducted with low- to mid-frequency transcranial ultrasound (60 to 300 kHz) (Daffertshofer, et al. 2005) (Nedelmann, et al. 2008). This transducer had a diameter of 64 mm and a focal length of 62.64 mm. The measured -3 dB focal volume dimensions were 4 mm laterally and 37 mm axially. It was driven by a function generator (3325DA, Agilent Technologies Inc., Santa Clara, CA, USA) and connected to a power amplifier (A300, Electronics & Innovation Ltd., Rochester, NY, USA) with a custom-made impedance matching network (Sonic Concepts). The clot was exposed for 60 min to 5 x 10^4 cycle bursts at a 0.2 Hz pulse repetition frequency, corresponding to a 2% duty cycle. The peak rarefactional pressure at the focus was set to 630 kPa, measured in the absence of the clot and vessel with a calibrated fibre optic hydrophone (Precision Acoustics, Dorchester, UK).

Passive cavitation detection (PCD) of acoustic emissions was carried out using a focused, circular, single-element, 7.5 MHz transducer (Panametrics V320-SU, Olympus Inc., Waltham, MA, USA). This PCD transducer had a focal length of 75 mm, an aperture of 12.5 mm, and -3 dB focal volume dimensions of and 1.2 mm laterally and 37.6 mm axially. Before each experiment, the foci of the 0.5 MHz and the PCD transducers were aligned with the surface of the clot using the PCD transducer in pulse-echo mode. The PCD signal was acquired using a 2 MHz high-pass filter (Allen Avionics Inc., Mineola, NY, USA) to block signals at the

fundamental frequency. The filter was connected to a pre- amplifier to achieve x25 signal amplification (SR445A, Stanford Research Systems, Sunnyvale, CA, USA). The first 2 ms of each 100 ms pulse were then acquired into a binary file at 10^8 samples per second using a data acquisition card and control software written in LabView (National Instruments, Austin, TX, USA). As the microbubbles were constantly replenished in the flow chamber, cavitation was expected to be consistent throughout treatment. Signal acquisition was therefore triggered for every 10^{th} burst in order to reduce data volume.

Image acquisition

Lysis progress was assessed from the changes in clot diameter throughout treatment. Images of the clot were captured every 30 s using a digital camera. Clot outlines were detected off-line using custom-written code in Matlab, and the maximum depth of clot lysis (i.e. maximum change in diameter compared to baseline) was computed at each time point in a 3 mm wide window around the axis of the ultrasound transducer. Linear regression on the depth of lysis over the 60 min of treatment yielded the overall lytic rate. In the group with magnetic targeting, magnetic material gradually accumulated near the clot until it obstructed the view in the region of interest, so the regression was limited to the period before full obstruction (at least the first 20 images).

PCD signal processing

The acoustic emissions recorded during treatment were processed as follows. The first 90 µs of the burst were discarded to account for the acoustic time of flight from the 0.5 MHz

transducer to the focal region and back to the PCD transducer. The signal was zero padded and windowed using a Hann window and its power spectral density derived by Fast Fourier Transform. The total power emitted in the 2-5 MHz frequency range was computed by integrating the power spectral density over the corresponding frequency range. Acoustic emissions in the ultraharmonic range were computed by integrating the power spectral density over six consecutive frequency bands containing ultraharmonics (odd multiples of half the driving frequency) with central values ranging from 2.25 MHz to 4.75 MHz and widths of 25 kHz, which is of the order of the -3dB bandwidth of the driving transducer. Similarly, acoustic emissions in the broadband range were computed by integrating the power spectral density over six consecutive frequency bands located away from harmonic and ultraharmonic peaks, with centres in the 2.375-4.875 MHz range and widths of 25 kHz. Finally, tThe acoustic emissions thus computed for each burst were summed over the whole duration of treatment, yielding the total energy of acoustic emission for that treatment.

Histological analysis

After treatment completion, the clots were immersed in formalin, and fixed in paraffin. 5-µm slices were prepared and stained with eosin and haematoxylin. They were analysed in bright field microscopy (Ti Eclipse, Nikon Instruments Inc., NY, USA) using a x20 objective (S Plan Fluor EWLD, Nikon).

Clot debris analysis

Secondary embolism due to circulation of clot debris is a potential risk of sonothrombolysis. In order to assess clot debris size, 15 mL of effluent were collected halfway through treatment and immediately stored at -20°C. The samples were then defrosted for 12 hours at 4°C. This low temperature was maintained so as to inhibit the enzymatic activity of tPA, limiting further breakdown of the clot debris. 100 µL samples of the solution were analysed with an optical particle sizer (Accusizer 780, Particle Sizing Systems, Santa Barbara, CA, USA), designed to size particles between 0.5 and 400 µm. Three samples were analysed for each clot.

Statistics

Differences among experimental groups were analysed in Matlab using two-way ANOVA, with post hoc Tukey HSD testing for multiple comparisons between groups. Statistical significance was defined as $p<0.05$ (denoted by * in the figures). Data with greater significance ($p<0.01$) are denoted by **.

Results

Magnetic field characterisation

A numerical simulation was performed to map the magnetic field and the magnetic field gradient in the phantom vessel. As expected, the magnitudes of both were symmetrical about the Oxz plane (data not shown) but not about the Oyz plane (Figure 2), because of the orientation of the magnetisation vector. The magnet achieved strong fields and steep

gradients within the vessel. Both decreased rapidly with increasing distance from the upper vertex of the magnet.

It must however be noted that the numerical model breaks down in a region within about 1 mm away from the magnet. This is due to the approximation of the magnetic medium as a lattice of evenly distributed point dipoles, which is no longer valid in the short range. Precise estimation of the magnetic field in this narrow region is, however, not relevant to the present study, as the region is occupied by the clot and no microbubbles can be present. Magnetic targeting takes place in the liquid above the clot, where valid predictions can be made and, in a range of positions inside the channel from 1.5 to 10 mm from the magnet, predicted values for the magnetic field are within 0.38-0.08 T, while the magnetic field gradient varies from 140 to 12 T/m.

Magnetic microbubble retention

Figure 3 shows a photograph of the experimental flow model after injection of a bolus of microbubble stock solution into the flow, past a clot phantom. In the absence of a magnet and of ultrasound exposure (Figure 3a), the microbubbles float to the top of the flow chamber due to their buoyancy and do not come into contact with the clot phantom. In the presence of a magnet (Figure 3b), the magnetic material accumulates in a narrow region (~3 mm-wide) that coincides with the focus of the 0.5 MHz transducer. As the clot is narrower than the tube, Figure 3c shows that some magnetic material collects at the bottom of the flow chamber on either side of the clot, where its contribution to lysis will be limited. A substantial proportion of the magnetic material, however, accumulates at the target site, directly on top of the clot.

The proportion of microbubbles retained in the model is quantified in Figure 4. In the absence of a magnet, the total greyscale intensity remained constant in the focal region over the period of observation, indicating no change in the amount of magnetic material. On the other hand, total greyscale intensity increased rapidly in the presence of a magnetic field, confirming a large increase in local concentration.

Effect of magnetic targeting on lysis rates

Six clots were treated in each experimental group. Maximum depth of clot lysis was measured every 30 s over the 60 min of treatment. Linear regression was carried out on the maximum depth of lysis and yielded an acceptable fit on average over all experimental groups (R^2 = 0.75 ± 0.3). In the two experimental groups involving microbubbles, the linear fit was very good (R^2 = 0.95 ±0.04).

Figure 5 shows the rates of lysis in all four experimental groups. Negligible lysis was observed in the clots treated with tPA only or with tPA + US (1.3 ± 1.4 x 10^{-3} mm/min and 2.9 ± 2.8 x 10^{-3} mm/min respectively). Lysis rates were substantially increased in the presence of microbubbles (11.2 ± 4.1 x 10^{-3} mm/min with US + tPA + microbubbles, non-significant); they were further accelerated (x 3.3 on average) with a magnetic field (36.6 ± 23.4 x 10^{-3} mm/min with US + tPA + microbubbles + magnet, $p<0.05$).

The effect of treatment on clot structure was investigated on H&E stained clot samples (Figure 6). The surface of clots treated without microbubbles (Figure 6a. and b.) was smooth. On the clot treated with tPA with US, it was not possible to identify with precision the focal region. In the samples treated with US + tPA + microbubbles, the damaged region

has a smooth surface and several small areas of erythrocyte depletion (Figure 6 c., direction of US exposure shown by the black arrow). Closer inspection shows that these cavities still contain fibrin. These observations are in agreement with a recent report by Petit et al. (2012). All of the samples treated with US + tPA + microbubbles + magnet were entirely lysed at the transducer focus after 60 minutes of treatment. Figure 6d shows the remaining clot fragments on either side of the lysed region. Numerous erythrocyte-depleted cavities with accumulation of magnetic material are present throughout the clot. Please note that in this case the clot was severed in two by the treatment. The left hand section shows the lysed region. The right hand section was not in the ultrasound focal region.

Effect of magnetic targeting on acoustic emissions

The acoustic emissions from the ultrasound focal region were monitored throughout treatment. As evidenced by the illustrative frequency-domain traces of acoustic emissions presented in Figure 7, the acoustic emissions observed under excitation conditions of 0.5 MHz and a peak rarefactional pressure of 630 kPa are primarily broadband in nature, which is consistent with previous investigations (Arvanitis, et al. 2011). To that end, no effort was made to separate broadband from narrowband emissions and the total energy of acoustic emissions can be taken as indicative of inertial cavitation.

Figure 7 further shows the mean and standard deviation of the total energy emitted in three frequency ranges: in the 2-5 MHz range, the ultraharmonic emissions (odd multiples of half the driving frequency), and broadband emissions. the 2-5 MHz frequency range for each experimental group.

In the US + tPA only group, ultraharmonic emissions dominated. The average energy emitted in the ultraharmonic range was 1.7 times the average energy in the broadband range. In the groups treated with microbubbles, the emissions were a combination of ultraharmonics and broadband noise. In both groups, the average energy emitted in the ultraharmonic range was 1.03 times the average energy in the broadband range.

In all three frequency ranges investigated, theThe use of microbubbles was associated with a significant increase in acoustic emissions over the US + tPA group ($p < 0.01$). In addition, there was a significant increase in acoustic emissions with US + tPA + microbubbles + magnet over US + tPA + microbubbles ($p < 0.01$). This validates the hypothesis that magnetic targeting enhances cavitation energy in the focal region by increasing the concentration of cavitation nuclei.

Investigating the potential of acoustic treatment monitoring

Acoustic emissions in the focal region were investigated as a potential indicator of treatment success. Lysis rates were plotted against acoustic emissions in the 2-5 MHz range (Figure 8). There was found to be a positive correlation between acoustic emissions and lysis rates. Linear fitting yielded a coefficient of $R^2 = 0.870$ with $p< 0.01$. It was deemed that there were insufficient data to fit more complex curves.

Clot debris

The effluent was collected during treatment and analysed. In all experimental groups, over 99.9% of the particles were smaller than 10 μm, i.e. of similar size to red blood cells, indicating that the risk of downstream embolisation with this treatment is low.

Discussion

In this study, magnetic targeting was associated with a significant increase in cavitation energy near the clot, confirming previous reports that magnetically targeted microbubbles can locally enhance cavitation (Crake, et al. 2015). As this enhanced cavitation was associated with accelerated clot lysis, this study demonstrates that magnetic targeting has the potential for a doubly positive impact on thrombolysis. Firstly, it may accelerate vessel recanalisation, increasing tissue salvage, and limiting the adverse side-effects associated with prolonged ultrasound exposure. These findings are particularly promising in the context of ischaemic stroke therapy, where early tissue reperfusion is crucial to improve patient outcomes (Rha and Saver 2007). Secondly, stronger cavitation signals may facilitate real-time treatment monitoring and thus enhance patient safety.

To the best of the authors' knowledge, this is the first report of magnetically targeted microbubbles as a method to accelerate sonothrombolysis. Targeted sonothrombolysis has been previously investigated *in vitro* and *in vivo* using various "biological" microbubble targeting methods (e.g. antibody conjugation) (Alonso, et al. 2009, Chen, et al. 2009, Culp, et al. 2004, Wu, et al. 1998, Xie, et al. 2009). Higher plasma D-dimer levels have been reported in rats treated with pulsed 2-MHz ultrasound and platelet-specific, abciximab-coated immunobubbles, compared to the non-specific immunobubble control group. Histological analysis also showed clot disintegration in 4/5 clots in the target group,

compared to 1/5 in the controls (Alonso, et al. 2009). (Xie, et al. 2009) investigated glycoprotein IIb/IIIa–targeted microbubbles in a porcine model of arterial thrombosis, in the presence of prourokinase. The authors showed that, compared to control microbubbles, the targeted bubbles were associated with significantly greater replenishment of contrast agents in the at-risk area of the myocardium after 15 min of treatment. Alternative approaches to biologically targeted sonothrombolysis have also utilised other ultrasound responsive particles. (Tiukinhoy-Laing, et al. 2007) have developed fibrin-targeted, tPA-loaded echogenic liposomes. When exposed to 120 kHz ultrasound, these particles achieved more effective thrombolysis *in vitro* than free tPA + US. In comparison to these biologically targeted agents, the main advantage of magnetically targeted microbubbles is the relatively long potential working distance: magnetically targeted agents do not need to be initially in contact with the target to be retained. This property is particularly relevant in the context of thrombosed vessels, which are characterised by reduced blood flow and complex haemodynamic patterns (Strony, et al. 1993, Wootton and Ku 1999).

Other researchers have provided an *in vitro* proof-of-concept for magnetically targeted enzymatic sonothrombolysis, developing magnetic polymer microparticles that release tPA upon exposure to very low frequency ultrasound (Kaminski, et al. 2008, Torno, et al. 2008). The present study uses magnetic microbubbles, which have the added advantage of strongly promoting cavitation. The microbubbles were effectively retained against physiological flow rates using a magnetic field within the 8 – 3.8 $x10^{-2}$ T range, and a 12-140 T/m magnetic field gradient. Such flux density and flux density gradients are achievable with permanent magnet arrays at depths up to a few tens of mm in the body depending on the flow rate (Barnsley, et al. 2015, Barnsley, et al. 2016, Owen, et al. 2015). This is sufficient for treating

clots in the middle cerebral artery (Gillard, et al. 1986), one of the brain vessels most commonly affected by ischaemic stroke (Demchuk, et al. 2001).

The results of this study suggest that sonothrombolysis can enable a reduction in the quantity of drug required. The drug alone did not produce significant lysis, which is attributable to the relatively short time frame of the experiment (60 min), to the low concentration of tPA (0.75 μg/mL) compared to clinical doses, and to the use of porcine blood and plasma (Huang, et al. 2017). Even under these conditions, substantial lysis acceleration occurred with ultrasound and non-targeted microbubbles. This is in agreement with previous studies that reported the possibility of lowering administered drug doses when using ultrasound and microbubbles (Brown, et al. 2011, Petit, et al. 2012). For instance, Brown *et al.* demonstrated *in vitro* that with pulsed 1 MHz ultrasound and albumin/dextrose microbubbles, tPA concentration could be reduced up to five times while maintaining thrombolytic efficacy. These results are encouraging in terms of patient safety, as lower doses of tPA could reduce the risk of intracranial haemorrhage in acute stroke management.

The results also demonstrate the feasibility of non-invasive treatment monitoring using passive cavitation detection, with good correlation between lysis rates and acoustic emissions. This contrasts with a previous study, in which whole porcine blood clots were exposed to tPA, pulsed ultrasound and lipid-shelled microbubbles (Datta, et al. 2008). The authors reported a strong correlation between final clot lysis and ultraharmonic emissions (R^2 = 0.83, $p<0.001$), and no correlation between lysis and broadband emissions. In the

acoustic conditions reported (120 kHz, 320 kPa, no flow), however, most of the emissions occurred in the harmonic and ultraharmonic range, whereas in the present study, the emissions occurred primarily in the broadband range. These findings suggest that the frequency range providing the most useful indicator of lytic success may depend upon the cavitation regime in the focal region and on the ratio between the wavelength and the mean bubble size. This is an area of active research (Porter, et al. 2017) (Bader, et al. 2015) (Petit, et al. 2015), needing further investigation.

The finding that sonothrombolysis can be significantly enhanced in an inertial cavitation regime warrants further discussion both in terms of potential mechanism and in terms of safety. Mechanistically, microstreaming has been routinely associated with non-inertial cavitation, primarily because of the need for persistent cavitation to occur in order for a stable microstreaming field to be established. However, several recent studies in the context of cancer drug delivery have indicated that suitably nucleated, sustained inertial cavitation in fact results in higher streaming velocities than non-inertial cavitation in vitro (Rifai, et al. 2010) and enables significantly enhanced drug delivery, penetration and distribution in vivo (Arvanitis, et al. 2011). These recent findings suggest that strategies which enable sustained inertial cavitation to occur, such as the magnetic retention approach presented here, could offer significant enhancements in terms of drug transport and penetration.

In terms of safety, inertial cavitation has traditionally been deemed undesirable for diagnostic and therapeutic applications, in great part due to reports of a higher incidence of unwanted bioeffects (Schafer, et al. 2005). Over the past decade, studies specifically aimed at opening the blood brain barrier have further indicated that inertial cavitation can cause

undesirable erythrocyte extravasation and cell death in murine brain models (McDannold, et al. 2006). However, a recent clinical study of opening the blood-brain-barrier in humans (Carpentier, et al. 2016) reported no safety concerns at peak rarefactional pressure amplitudes of up to 1.1 MPa at a frequency of 1.05 MHz, which would result in inertial cavitation in the presence of microbubbles. A key feature of this clinical study was that the ultrasound excitation was highly localized through a transcranially implanted probe, even though both the microbubbles and the drug were systemically administered. Similarly, it is conceivable that an approach which localizes and only locally enhances inertial cavitation could ultimately present a clinically acceptable safety profile.

Limitations

The study has a number of limitations that warrant comment. The model mimics a partial vessel occlusion, which does not perfectly represent most *in vivo* pathological thrombi, although partial occlusions may also lead to acute clinical symptoms (Chesebro, et al. 1987, Xie, et al. 2009). A single vessel orientation (horizontal) was investigated in the present study; future work may focus on the effect of different orientation angles, in order to mimic a broader range of clinical and physiological conditions. Also, blood from a single animal was used in the results presented here. The range of hematocrits in the porcine blood donors used for the current work was consistently found to be in the range 25 – 30 % and clots were assigned to individual groups blindly in order to mitigate the possibility of bias. Nevertheless, in future studies, samples from multiple animals may be pooled in order to limit the effects of pig-to-pig variability. To further increase clinical relevance, the composition of the plasma solution in the flow loop may also be improved. A recent study by Huang et al. (2017) demonstrated that using human plasminogen in the liquid surrounding a porcine clot produces

sonothrombolysis behaviours that resemble more closely human clots in human plasma.

In addition, many published studies use travelling waves when studying sonothrombolysis (Datta, et al. 2006, Petit, et al. 2012, Pfaffenberger, et al. 2005, Xie, et al. 2009), while the ultrasound field in this study included a partial standing wave. This is inherent to the geometry of the setup. It is not expected to affect microbubble oscillations, as the size of a microbubble (~1-10 μm) is much smaller than half the wavelength at 0.5 MHz (~1.5mm), but it may have affected microbubble translation. In clinical applications, standing waves are generally not desirable for patient safety (Baron, et al. 2009, Daffertshofer, et al. 2005), although standing waves may also form *in vivo* in transcranial applications (Baron, et al. 2009, Bouchoux, et al. 2014). Furthermore, the microbubble formulation used was not optimal for human use due to its composition. Magnetic microbubble formulations with improved biocompatibility have recently been developed and characterized, and will be used in future work (Owen, et al. 2012). Finally, the physical properties of the flow medium did not faithfully replicate blood's properties, which may impact on microbubble flow behaviour and acoustic response. Future studies will be conducted using whole blood, which may require changes to the optical imaging technique employed to quantify clot lysis (because of the reduced image quality).

Conclusions

This study demonstrates *in vitro* that magnetic targeting can significantly accelerate microbubble-enhanced enzymatic sonothrombolysis at 0.5 MHz, with the potential to reduce administered drug doses and to achieve faster vessel recanalisation. A more than 3 fold increase in the lysis rate was observed when using magnetic targeting, compared with microbubbles in the absence of magnetic force. The total energy of acoustic emissions was

strongly correlated with lytic rates, providing a possible method for real-time treatment monitoring. These results indicate that magnetic targeting has the potential to enhance treatment efficacy and patient safety in the management of occlusive conditions using microbubble mediated sonothrombolysis.

Acknowledgements

The authors gratefully acknowledge the assistance of Paul Lyon and Murali Somasundaram in the blood collection process. They are also indebted to Jim Fisk and David Salisbury for their skilful fabrication of the flow setup; and to Richard Stillion for his advice on the clot histopathology. The work was supported by funding from the Research Council UK Digital Economy Programme, through the Centre for Doctoral Training in Healthcare Innovation (grant number EP/G036861/1) and the Engineering and Physical Sciences Research Council (EPSRC grant number EP/I021795/1).

References

Alkatheri A. Stability of Recombinant Tissue Plasminogen Activator at -30 degrees C over One Year. Pharmaceuticals 2013; 6:25-31.

Alonso A, Dempfle CE, Della Martina A, Stroick M, Fatar M, Zohsel K, Allemann E, Hennerici MG, Meairs S. In vivo clot lysis of human thrombus with intravenous abciximab immunobubbles and ultrasound. Thromb Res 2009; 124:70-74.

American College of Emergency Physicians, American Academy of Neurology. Clinical Policy: Use of intravenous tPA for the management of acute ischemic stroke in the emergency department. Annals of emergency medicine 2013; 61:225-43.

Arvanitis CD, Bazan-Peregrino M, Rifai B, Seymour LW, Coussios CC. Cavitation-enhanced extravasation for drug delivery. Ultrasound in medicine & biology 2011; 37:1838-52.

Bader KB, Gruber MJ, Holland CK. Shaken and stirred: mechanisms of ultrasound-enhanced thrombolysis. Ultrasound in medicine & biology 2015; 41:187-96.

Barber PA, Zhang J, Demchuk AM, Hill MD, Buchan AM. Why are stroke patients excluded from TPA therapy? An analysis of patient eligibility. Neurology 2001; 56:1015-20.

Barnsley LC, Carugo D, Owen J, Stride E. Halbach arrays consisting of cubic elements optimised for high field gradients in magnetic drug targeting applications. Phys Med Biol 2015; 60:8303-27.
Barnsley LC, Carugo D, Stride E. Optimized shapes of magnetic arrays for drug targeting applications. J Phys D Appl Phys 2016; 49.
Baron C, Aubry JF, Tanter M, Meairs S, Fink M. Simulation of intracranial acoustic fields in clinical trials of sonothrombolysis. Ultrasound in medicine & biology 2009; 35:1148-58.
Bouchoux G, Shivashankar R, Abruzzo TA, Holland CK. In silico study of low-frequency transcranial ultrasound fields in acute ischemic stroke patients. Ultrasound in medicine & biology 2014; 40:1154-66.
Brown AT, Flores R, Hamilton E, Roberson PK, Borrelli MJ, Culp WC. Microbubbles improve sonothrombolysis in vitro and decrease hemorrhage in vivo in a rabbit stroke model. Investigative radiology 2011; 46:202-7.
California Acute Stroke Pilot Registry Investigators. Prioritizing interventions to improve rates of thrombolysis for ischemic stroke. Neurology 2005; 64:654-9.
Carpentier A, Canney M, Vignot A, Reina V, Beccaria K, Horodyckid C, Karachi C, Leclercq D, Lafon C, Chapelon JY, Capelle L, Cornu P, Sanson M, Hoang-Xuan K, Delattre JY, Idbaih A. Clinical trial of blood-brain barrier disruption by pulsed ultrasound. Sci Transl Med 2016; 8:343re2.
Chen SC, Ruan JL, Cheng PW, Chuang YH, Liz PC. In Vitro Evaluation of Ultrasound-Assisted Thrombolysis Using a Targeted Ultrasound Contrast Agent. Ultrasonic Imaging 2009; 31:235-46.
Chesebro JH, Knatterud G, Roberts R, Borer J, Cohen LS, Dalen J, Dodge HT, Francis CK, Hillis D, Ludbrook P, Markis JE, Mueller H, Passamani ER, Powers ER, Rao AK, Robertson T, Ross A, Ryan TJ, Sobel BE, Willerson J, Williams DO, Zaret BL, Braunwald E. Thrombolysis in Myocardial-Infarction (Timi) Trial, Phase-I - a Comparison between Intravenous Tissue Plasminogen-Activator and Intravenous Streptokinase - Clinical Findings through Hospital Discharge. Circulation 1987; 76:142-54.
Crake C, Saint Victor MD, Owen J, Coviello C, Collin J, Coussios CC, Stride E. Passive acoustic mapping of magnetic microbubbles for cavitation enhancement and localization. Phys Med Biol 2015; 60:785-806.
Culp WC, Porter TR, Lowery J, Xie F, Roberson PK, Marky L. Intracranial clot lysis with intravenous microbubbles and transcranial ultrasound in swine. Stroke 2004; 35:2407-11.
Daffertshofer M, Gass A, Ringleb P, Sitzer M, Sliwka U, Els T, Sedlaczek O, Koroshetz WJ, Hennerici MG. Transcranial low-frequency ultrasound-mediated thrombolysis in brain ischemia: increased risk of hemorrhage with combined ultrasound and tissue plasminogen activator: results of a phase II clinical trial. Stroke 2005; 36:1441-6.
Datta S, Coussics CC, Ammi AY, Mast TD, de Courten-Myers GM, Holland CK. Ultrasound-enhanced thrombolysis using Definity (R) as a cavitation nucleation agent. Ultrasound in Medicine and Biology 2008; 34:1421-33.
Datta S, Coussios CC, McAdory LE, Tan J, Porter T, De Courten-Myers G, Holland CK. Correlation of cavitation with ultrasound enhancement of thrombolysis. Ultrasound in Medicine and Biology 2006; 32:1257-67.
de Saint Victor M, Carugo D, Barnsley LC, Owen J, Coussios CC, Stride E. Magnetic targeting to enhance microbubble delivery in an occluded microarterial bifurcation. Phys Med Biol 2017; 62:7451-70.

570 Demchuk AM, Burgin WS, Christou I, Felberg RA, Barber PA, Hill MD, Alexandrov AV.
571 Thrombolysis in brain ischemia (TIBI) transcranial Doppler flow grades predict
572 clinical severity, early recovery, and mortality in patients treated with intravenous
573 tissue plasminogen activator. Stroke 2001; 32:89-93.
574 Engel-Herbert R, Hesjedal T. Calculation of the magnetic stray field of a uniaxial magnetic
575 domain. J Appl Phys 2005; 97.
576 Feigin V, Norrving B, Mensah G. Global Burden of Stroke. Circ. Res. 2017; 120: 439-48.
577 FDA. Alteplase Product Approval Information. US Food and Drug Aministration Licensing
578 Action 1996; 6/18/96.
579 Gillard JH, Kirkham FJ, Levin SD, Neville BG, Gosling RG. Anatomical validation of
580 middle cerebral artery position as identified by transcranial pulsed Doppler
581 ultrasound. J Neurol Neurosurg Psychiatry 1986; 49:1025-9.
582 Hagisawa K, Nishioka T, Suzuki R, Maruyama K, Takase B, Ishihara M, Kurita A,
583 Yoshimoto N, Nishida Y, Iida K, Luo H, Siegel RJ. Thrombus-targeted
584 perfluorocarbon-containing liposomal bubbles for enhancement of ultrasonic
585 thrombolysis: invitro and invivo study. J Thromb Haemost 2013; 11:1565-73.
586 Hockham N, Coussios CC, Arora M. A Real-Time Controller for Sustaining Thermally
587 Relevant Acoustic Cavitation During Ultrasound Therapy. Ieee T Ultrason Ferr 2010;
588 57:2685-94.
589 Holland CK, Vaidya SS, Datta S, Coussios CC, Shaw GJ. Ultrasound-enhanced tissue
590 plasminogen activator thrombolysis in an in vitro porcine clot model. Thromb Res
591 2008; 121:663-73.
592 Hua X, Zhou L, Liu P, He Y, Tan K, Chen Q, Gao Y, Gao Y. In vivo thrombolysis with
593 targeted microbubbles loading tissue plasminogen activator in a rabbit femoral artery
594 thrombus model. Journal of thrombosis and thrombolysis 2014; 38:57-64.
595 Huang S, Shekhar H, Holland CK. Comparative lytic efficacy of rt-PA and ultrasound in
596 porcine versus human clots. PLoS One 2017; 12:e0177786.
597 Jaffe GJ, Green GDJ, Abrams GW. Stability of Recombinant Tissue Plasminogen-Activator.
598 Am J Ophthalmol 1989; 108:90-91.
599 Kaminski MD, Xie YM, Mertz CJ, Finck MR, Chen HT, Rosengart AJ. Encapsulation and
600 release of plasminogen activator from biodegradable magnetic microcarriers. Eur J
601 Pharm Sci 2008; 35:96-103.
602 Lu Y, Wang J, Huang R, Chen G, Zhong L, Shen S, Zhang C, Li X, Cao S, Liao W, Liao Y,
603 Bin J. Microbubble-Mediated Sonothrombolysis Improves Outcome After
604 Thrombotic Microembolism-Induced Acute Ischemic Stroke. Stroke 2016; 47:1344-
605 53.
606 McDannold N, Vykhodtseva N, Hynynen K. Targeted disruption of the blood-brain barrier
607 with focused ultrasound: association with cavitation activity. Phys Med Biol 2006;
608 51:793-807.
609 Meunier JM, Holland CK, Lindsell CJ, Shaw GJ. Duty cycle dependence of ultrasound
610 enhanced thrombolysis in a human clot model. Ultrasound in Medicine and Biology
611 2007; 33:576-83.
612 Molina CA, Ribo M, Rubiera M, Montaner J, Santamarina E, Delgado-Mederos R, Arenillas
613 JF, Huertas R, Purroy F, Delgado P, Alvarez-Sabin J. Microbubble administration
614 accelerates clot lysis during continuous 2-MHz ultrasound monitoring in stroke
615 patients treated with intravenous tissue plasminogen activator. Stroke 2006; 37:425-
616 29.
617 Naghavi M, et al. Global, regional, and national age-sex specific all-cause and cause-specific
618 mortality for 240 causes of death, 1990-2013: a systematic analysis for the Global
619 Burden of Disease Study 2013. Lancet 2015; 385: 117-71.

Nedelmann M, Brandt C, Schneider F, Eicke BM, Kempski O, Krummenauer F, Dieterich M. Ultrasound-induced blood clot dissolution without a thrombolytic drug is more effective with lower frequencies. Cerebrovasc Dis 2005; 20:18-22.
Nedelmann M, Reuter P, Walberer M, Sommer C, Alessandri B, Schiel D, Ritschel N, Kempski O, Kaps M, Mueller C, Bachmann G, Gerriets T. Detrimental Effects of 60 Khz Sonothrombolysis in Rats with Middle Cerebral Artery Occlusion. Ultrasound in Medicine and Biology 2008; 34:2019-27.
NICE. Stroke and transient ischaemic attack in over 16s : diagnosis and initial management. National Institute for Health and Care Excellence 2008; Clinical guideline [CG68].
Ogata T, Kimura K, Nakajima M, Ikeno K, Naritomi H, Minematsu K. Transcranial color-coded real-time sonographic criteria for occlusion of the middle cerebral artery in acute ischemic stroke. AJNR. American journal of neuroradiology 2004; 25:1680-4.
Owen J, Rademeyer P, Chung D, Cheng Q, Holroyd D, Coussios C, Friend P, Pankhurst QA, Stride E. Magnetic targeting of microbubbles against physiologically relevant flow conditions. Interface Focus 2015; 5.
Owen J, Zhou B, Rademeyer P, Tang MX, Pankhurst Q, Eckersley R, Stride E. Understanding the Structure and Mechanism of Formation of a New Magnetic Microbubble Formulation. Theranostics 2012; 2:1127-39.
Perren F, Loulidi J, Poglia D, Landis T, Sztajzel R. Microbubble potentiated transcranial duplex ultrasound enhances IV thrombolysis in acute stroke. Journal of thrombosis and thrombolysis 2008; 25:219-23.
Petit B, Bohren Y, Gaud E, Bussat P, Arditi M, Yan F, Tranquart F, Allemann E. Sonothrombolysis: the contribution of stable and inertial cavitation to clot lysis. Ultrasound in medicine & biology 2015; 41:1402-10.
Petit B, Gaud E, Colevret D, Arditi M, Yan F, Tranquart F, Allemann E. In vitro sonothrombolysis of human blood clots with BR38 microbubbles. Ultrasound in medicine & biology 2012; 38:1222-33.
Pfaffenberger S, Devcic-Kuhar B, Kollmann C, Kastl SP, Kaun C, Speidl WS, Weiss TW, Demyanets S, Ullrich R, Sochor H, Wober C, Zeitlhofer J, Huber K, Groschl M, Benes E, Maurer G, Wojta J, Gottsauner-Wolf M. Can a commercial diagnostic ultrasound device accelerate thrombolysis? An in vitro skull model. Stroke 2005; 36:124-28.
Porter TR, Xie F, Lof J, Powers J, Vignon F, Shi W, White M. The Thrombolytic Effect of Diagnostic Ultrasound-Induced Microbubble Cavitation in Acute Carotid Thromboembolism. Investigative radiology 2017; 52:477-81.
Rha JH, Saver JL. The impact of recanalization on ischemic stroke outcome - A meta-analysis. Stroke 2007; 38:967-73.
Rifai B, Arvanitis CD, Bazan-Peregrino M, Coussios CC. Cavitation-enhanced delivery of macromolecules into an obstructed vessel. J Acoust Soc Am 2010; 128:EL310-15.
Schafer S, Kliner S, Klinghammer L, Kaarmann H, Lucic I, Nixdorff U, Rosenschein U, Daniel WG, Flachskampf FA. Influence of ultrasound operating parameters on ultrasound-induced thrombolysis in vitro. Ultrasound in Medicine and Biology 2005; 31:841-47.
Schleicher N, Tomkins AJ, Kampschulte M, Hyvelin JM, Botteron C, Juenemann M, Yeniguen M, Krombach GA, Kaps M, Spratt NJ, Gerriets T, Nedelmann M. Sonothrombolysis with BR38 Microbubbles Improves Microvascular Patency in a Rat Model of Stroke. PLoS One 2016; 11:e0152898.
Sennoga CA, Mahue V, Loughran J, Casey J, Seddon JM, Tang M, Eckersley RJ. On sizing and counting of microbubbles using optical microscopy. Ultrasound in medicine & biology 2010; 36:2093-6.

Serrador JM, Picot PA, Rutt BK, Shoemaker JK, Bondar RL. MRI measures of middle cerebral artery diameter in conscious humans during simulated orthostasis. Stroke 2000; 31:1672-78.

Stride E, Porter C, Prieto AG, Pankhurst Q. Enhancement of microbubble mediated gene delivery by simultaneous exposure to ultrasonic and magnetic fields. Ultrasound in medicine & biology 2009; 35:861-8.

Strony J, Beaudoin A, Brands D, Adelman B. Analysis of Shear-Stress and Hemodynamic Factors in a Model of Coronary-Artery Stenosis and Thrombosis. Am J Physiol 1993; 265:H1787-H96.

Tiukinhoy-Laing SD, Buchanan K, Parikh D, Huang SL, MacDonald RC, McPherson DD, Klegerman ME. Fibrin targeting of tissue plasminogen activator-loaded echogenic liposomes. J Drug Target 2007; 15:109-14.

Torno MD, Kaminski MD, Xie YM, Meyers RE, Mertz CJ, Liu X, O'Brien WD, Rosengart AJ. Improvement of in vitro thrombolysis employing magnetically-guided microspheres. Thromb Res 2008; 121:799-811.

Wootton DM, Ku DN. Fluid mechanics of vascular systems, diseases, and thrombosis. Annu Rev Biomed Eng 1999; 1:299-329.

Wu YQ, Unger EC, McCreery TP, Sweitzer RH, Shen DK, Wu GL, Vielhauer MD. Binding and lysing of blood clots using MRX-408. Investigative radiology 1998; 33:880-85.

Xie F, Lof J, Everbach C, He AM, Bennett RM, Matsunaga T, Johanning J, Porter TR. Treatment of Acute Intravascular Thrombi With Diagnostic Ultrasound and Intravenous Microbubbles. Jacc-Cardiovasc Imag 2009; 2:511-18.

Xie F, Lof J, Matsunaga T, Zutshi R, Porter TR. Diagnostic Ultrasound Combined With Glycoprotein IIb/IIIa-Targeted Microbubbles Improves Microvascular Recovery After Acute Coronary Thrombotic Occlusions. Circulation 2009; 119:1378-85.

Figure captions

Figure 1: Overview of the experimental setup. The clot (1) was placed in an acoustically and optically transparent chamber through which a dilute plasma solution (1.25% v/v in PBS) was flowing. tPA and microbubbles were continuously injected into the flow by an infusion pump (2). A magnet (3) enabled magnetic retention of the microbubbles at the clot site. Ultrasound exposure and acoustic monitoring were performed by a pair of coaxial transducers (0.5 MHz and 7.5 MHz respectively) (4). Lysis progress was monitored using a digital camera (5).

Figure 2: Simulated contours of the magnetic field created by the magnet in the axial plane of the flow chamber; a) magnitude of magnetic field, **B**; b) magnitude of magnetic field gradient, $\nabla\mathbf{B}$. Inset (above): origin, orientation of the axes, and magnetisation vector (yellow arrow). The y-axis points into the page.

Figure 3: Magnetic microbubble retention in the experimental setup. Magnetic microbubbles (brown suspension at the top of the channel) flowing past a model clot (light-coloured cylinder at the bottom of the channel) in the absence and in the presence of a magnet. a) front view, control. ROI is the region of interest for image analysis; b) front view, enlarged, with magnet; c) top view, with magnet. For reference the length of each side of the magnet was 12.7 mm.

Figure 4: Accumulation of magnetic material in the focal region of the 0.5 MHz transducer over 12 s with (red line) and without (blue line) magnetic targeting (n =3). A 1 mL bolus of the microbubble stock solution was injected into the flow and images were acquired at 30 frames/second following the procedure described in the methods section. Normalised retention at a given time point t is defined as the total greyscale intensity in the ROI at this time point, divided by the total greyscale intensity at t = 0. Error bars represent the range of values observed.

Figure 5: Lysis rates during enzymatic sonothrombolysis of retracted porcine clots with magnetically targeted microbubbles (n=6). The clots were treated with tPA (0.75 µg/mL), 0.5 MHz ultrasound, 630 kPa peak rarefactional pressure, a 0.2 Hz pulse repetition frequency and a 2% duty cycle. Maximum depth of clot lysis was computed on photographs taken every 30 s during treatment, yielding the lysis rate. Error bars represent standard deviations from the mean. Significance (* = $p<0.05$) was calculated by ANOVA with Tukey post hoc test.

Figure 6: Histological samples of porcine clots after enzymatic thrombolysis. The clots were treated for 60 minutes with a) tPA (0.75 µg/mL) only; b) tPA and 0.5 MHz ultrasound (direction of propagation: black arrows), 630 kPa peak rarefactional pressure, a 0.2 Hz pulse repetition frequency and a 2% duty cycle; c) tPA, ultrasound and magnetic microbubbles in the absence of a magnetic field; d) tPa, ultrasound and magnetic microbubbles in the presence of a magnetic field. The clots were fixed in formalin, embedded in paraffin and stained with eosin and haematoxylin. The striations seen in panels a and c are thought to have been produced during sectioning of the clot by the serrated edge of the blade used.

741 **Figure 7**: Acoustic energy detected during sonothrombolysis of retracted porcine clots with
742 magnetically targeted microbubbles (n = 6). The clots were treated with tPA (0.75 μg/mL),
743 0.5 MHz ultrasound, 630 kPa peak rarefactional pressure, a 0.2 Hz pulse repetition
744 frequency and a 2% duty cycle. The acoustic emissions at the focus were acquired with a 7.5
745 MHz PCD transducer mounted coaxially with the 0.5 MHz transducer. Error bars represent
746 standard deviations from the mean. a) total energy in the 2 – 5 MHz frequency range;
747 Significance (** = $p<0.01$) was calculated by two-way ANOVA with Tukey post hoc test; b)
748 illustrative frequency-domain trace of received acoustic emissions in the t-PA+ US group; c)
749 illustrative frequency-domain trace of received acoustic emissions in the t-PA+ US+ MB
750 group; d) illustrative frequency-domain trace of received acoustic emissions in the t-PA+
751 US+ MB + Magnet group. The green and red rectangles respectively frame 25 kHz-wide
752 ultraharmonic and broadband regions, illustrating that the emissions are primarily
753 broadband in nature.

754 **Figure 8**: Bivariate representation of lysis rate and total acoustic energy detected in the 2-5
755 MHz range. The clots were treated with tPA (0.75 μg/mL), 0.5 MHz ultrasound, 630 kPa peak
756 rarefactional pressure, a 0.2 Hz pulse repetition frequency and a 2% duty cycle. Maximum
757 depth of clot lysis was computed on photographs taken every 30 s during treatment,
758 yielding the lysis rate. The acoustic emissions at the focus were acquired with a 7.5 MHz
759 PCD transducer mounted coaxially with the 0.5 MHz transducer.

760

fig1-setup.tif
Click here to download high resolution image

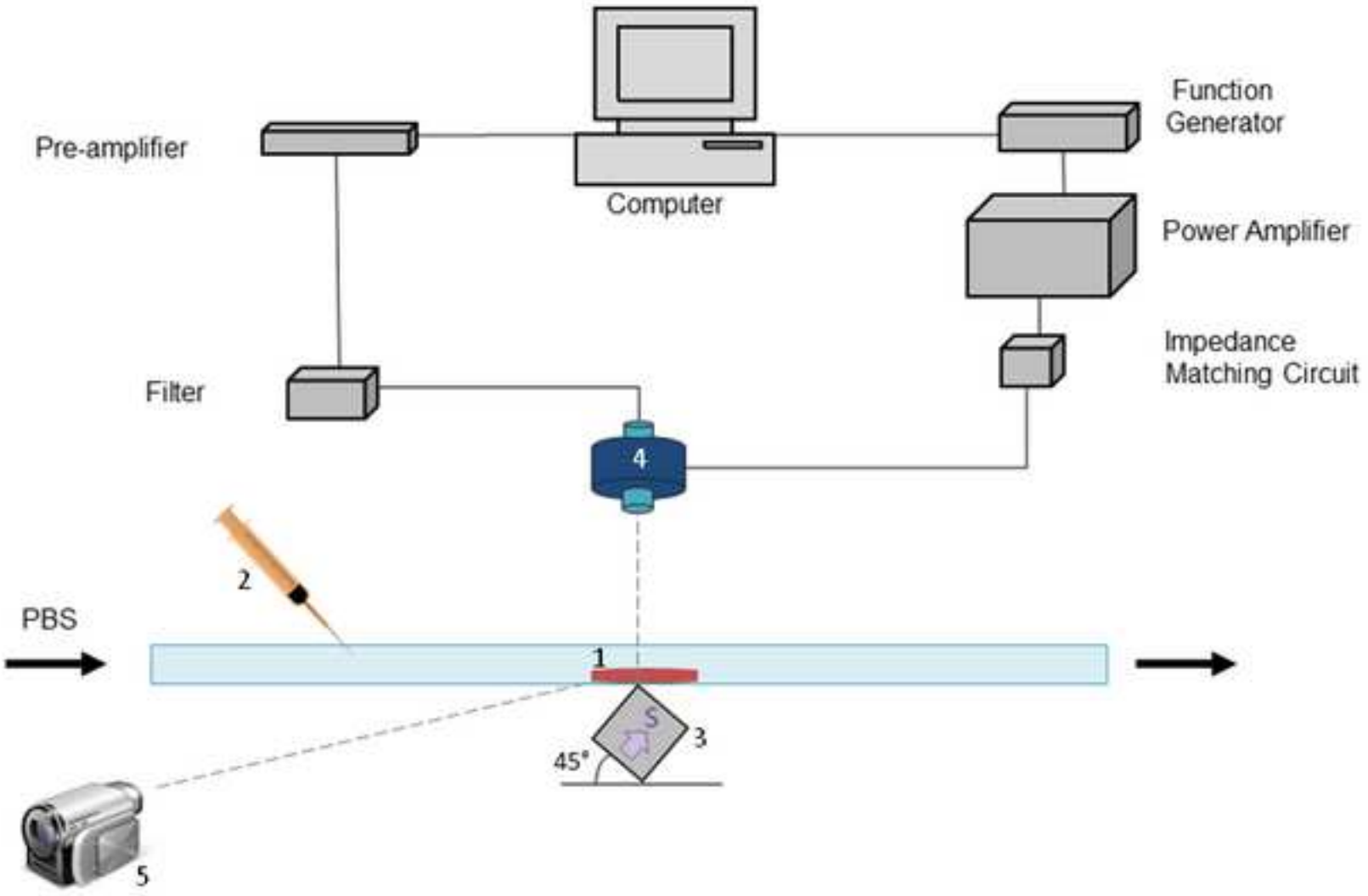

fig2 -magneticfield.tif

Click here to download high resolution image

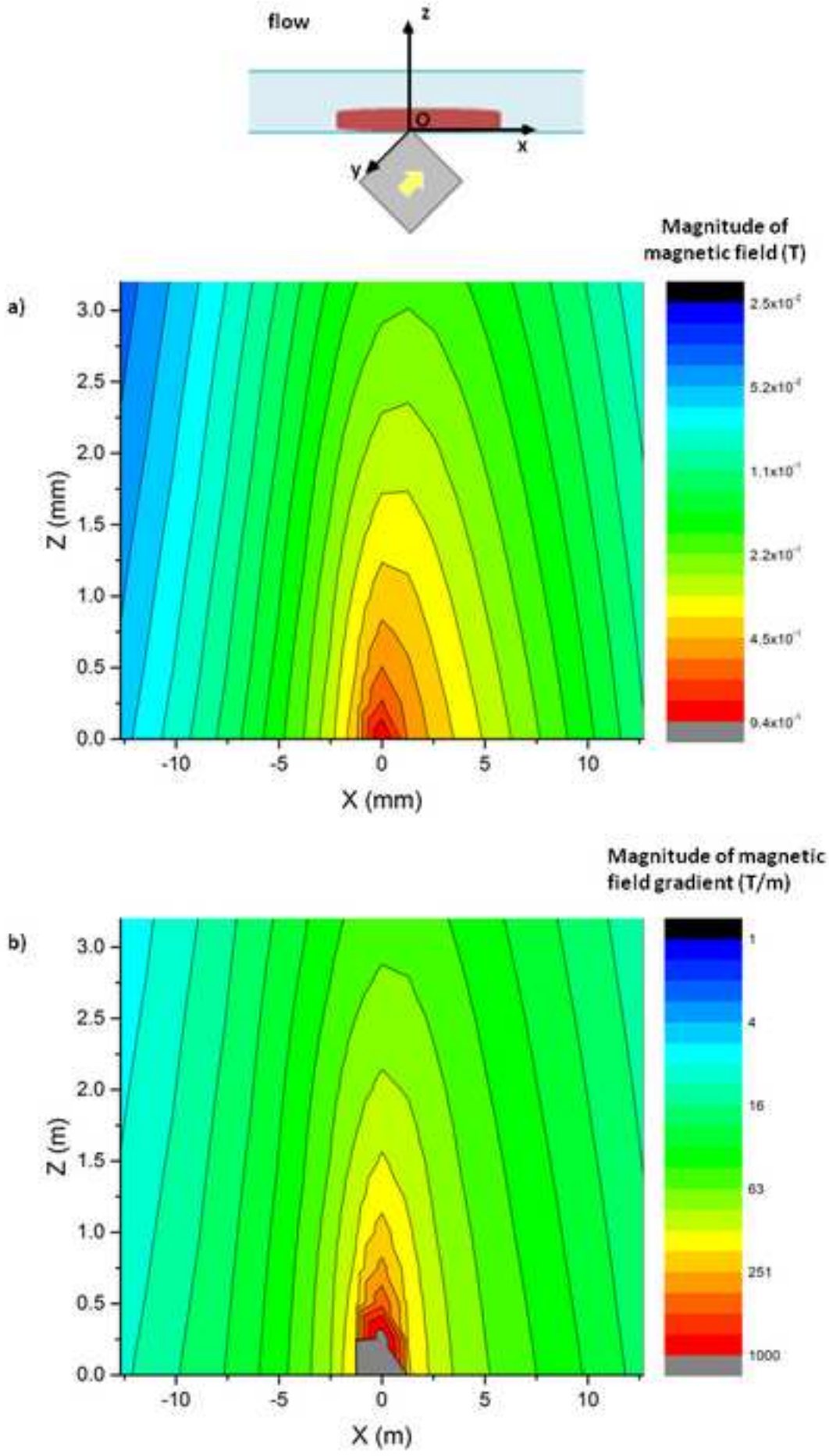

fig3 -magnetevidence.tif
Click here to download high resolution image

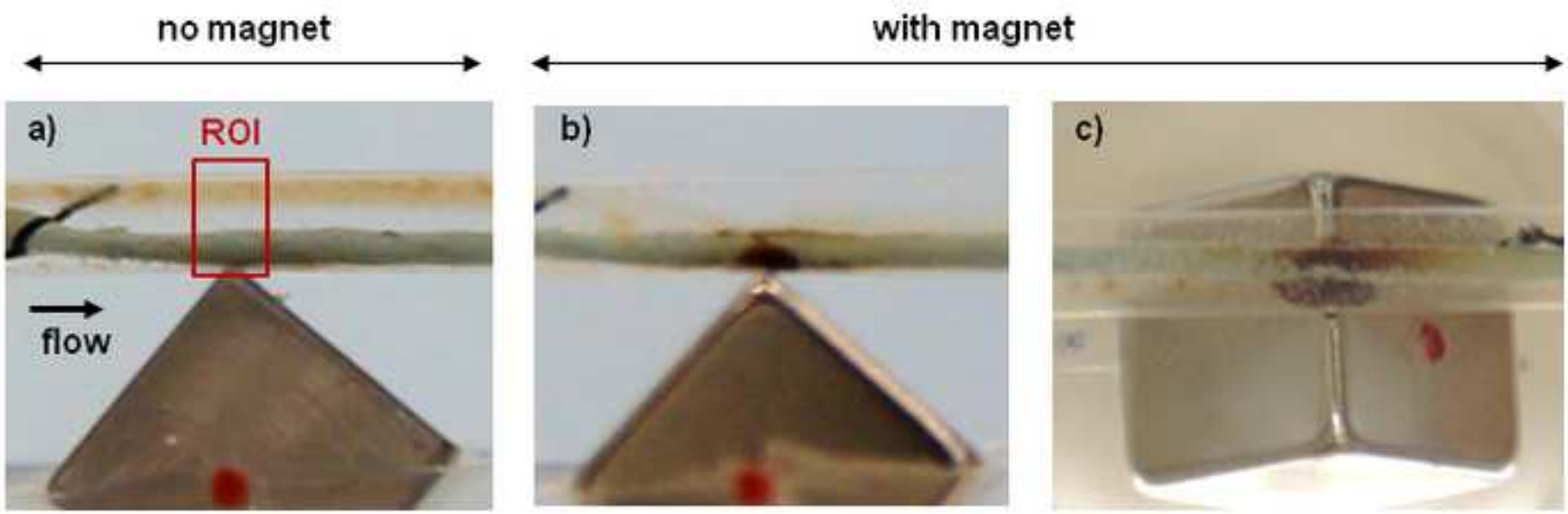

fig4-accumulation.tif
Click here to download high resolution image

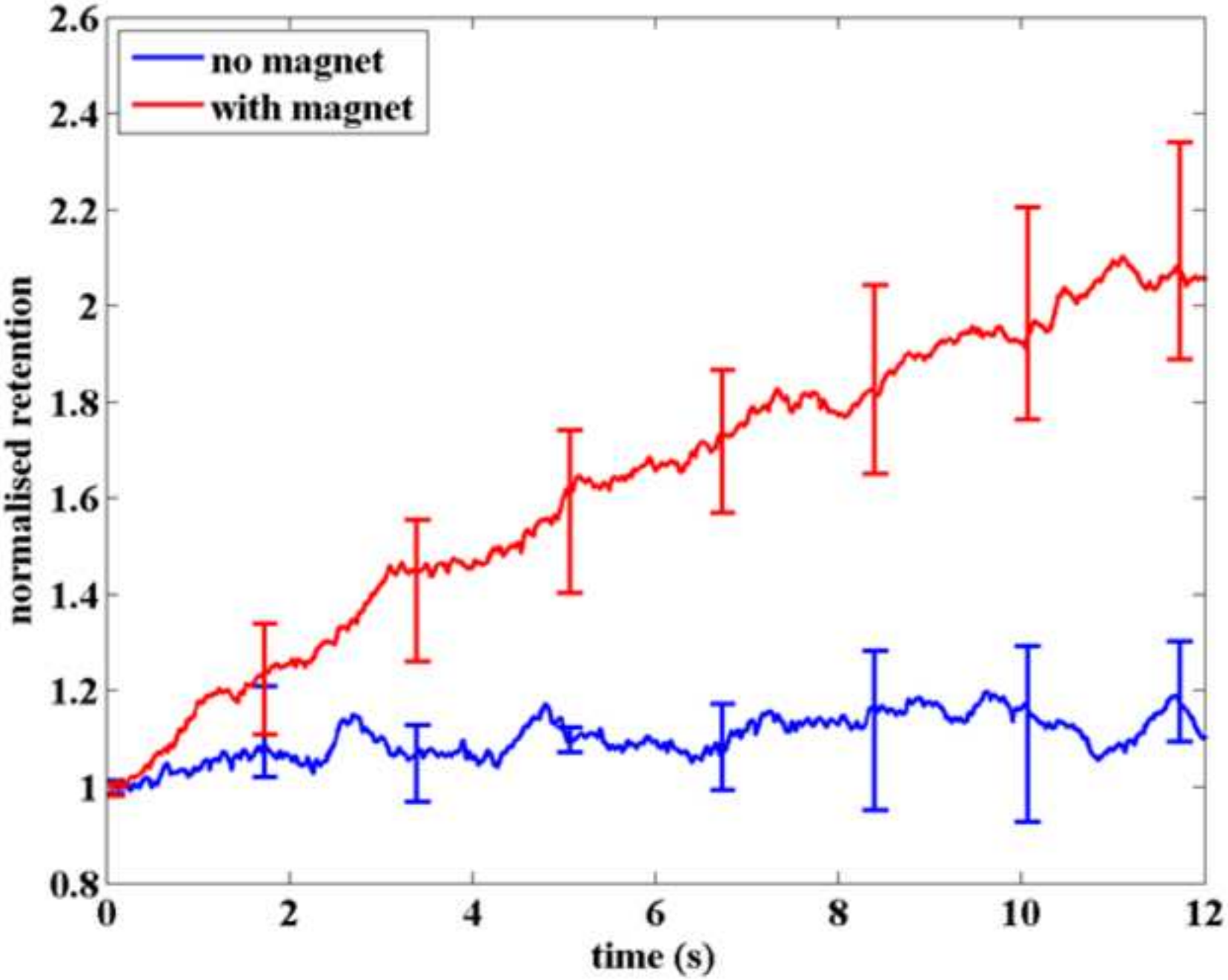

fig5-lysis.tif
Click here to download high resolution image

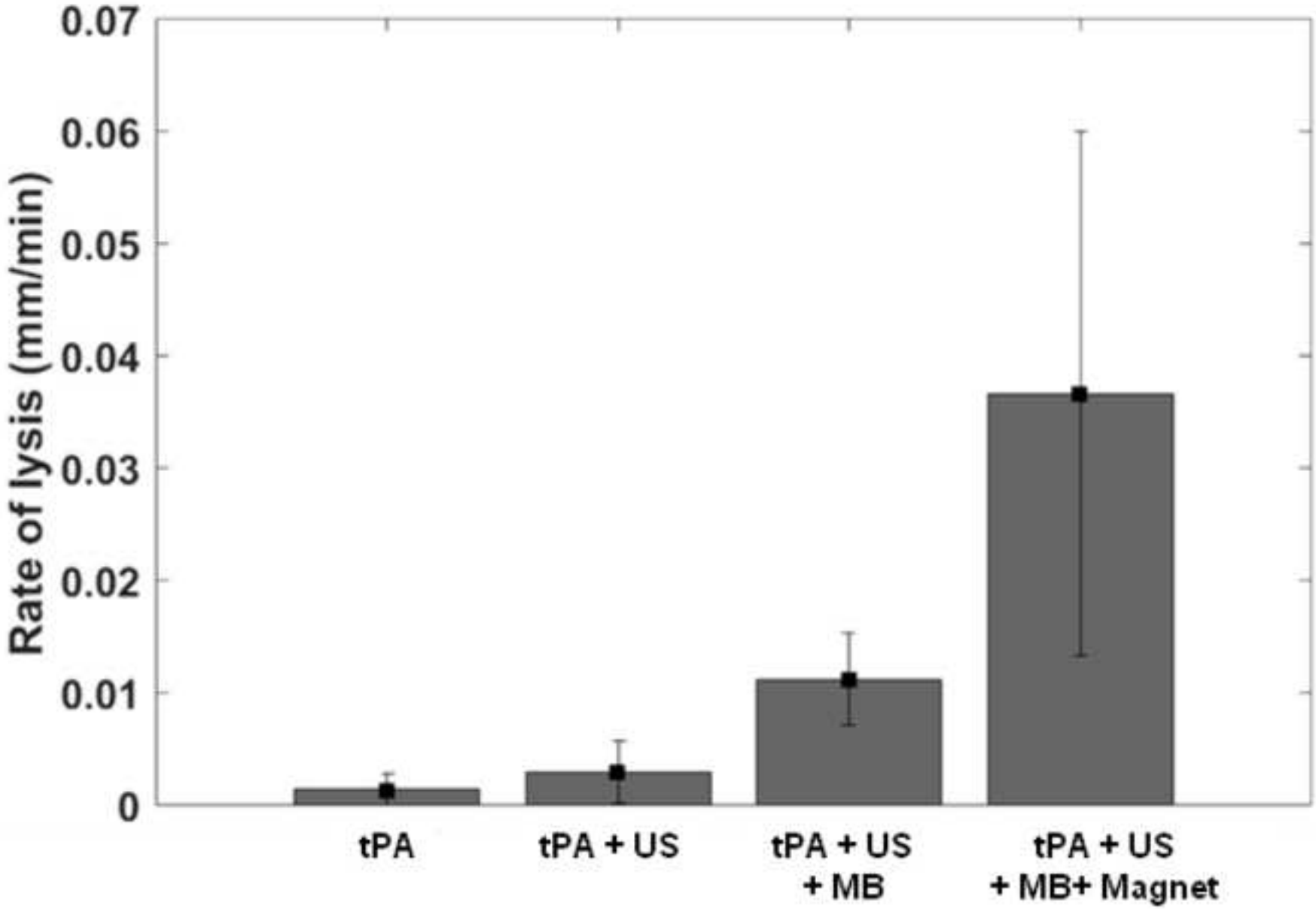

fig6-histology.tif
Click here to download high resolution image

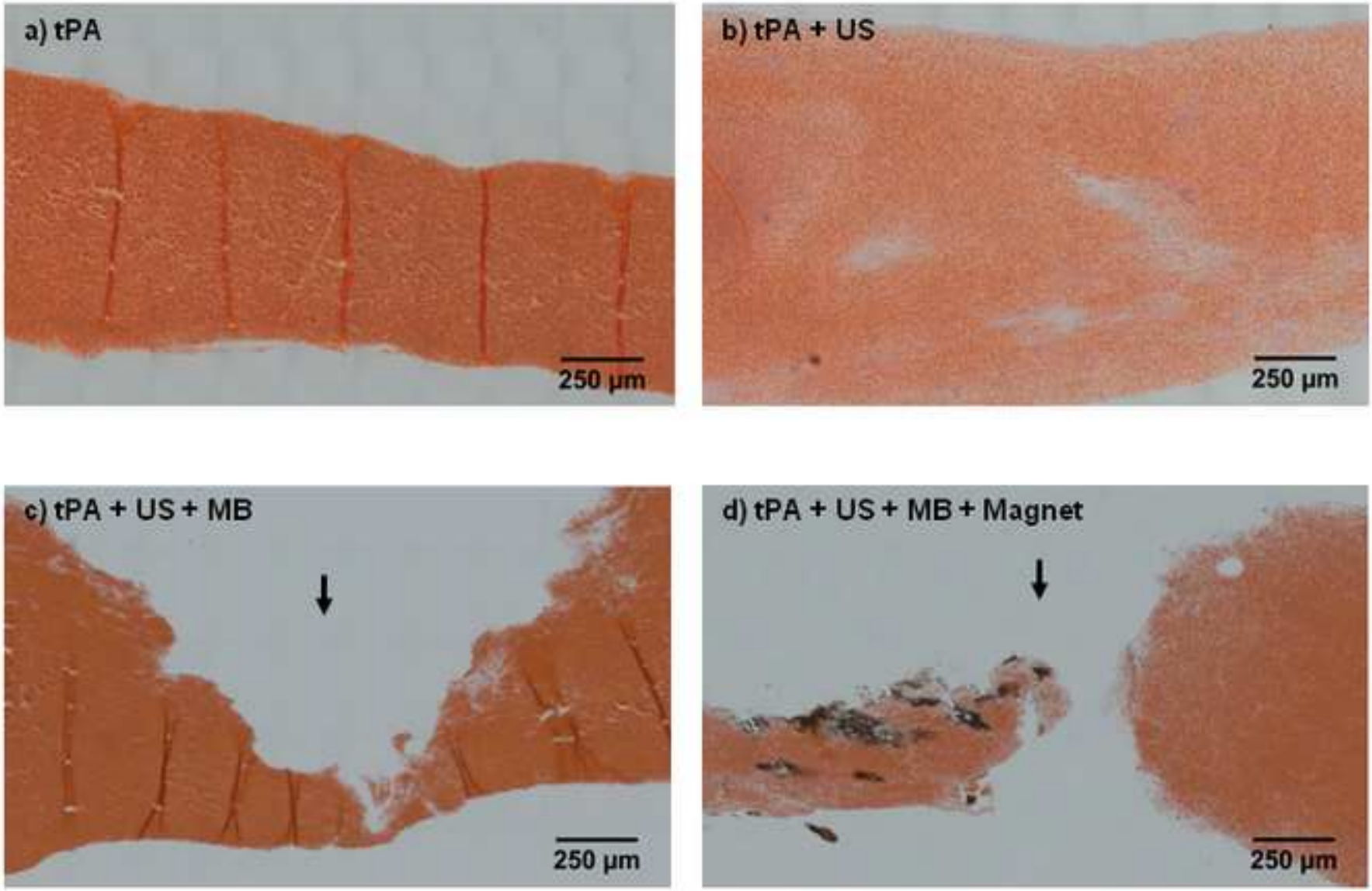

Figure 7

Click here to download high resolution image

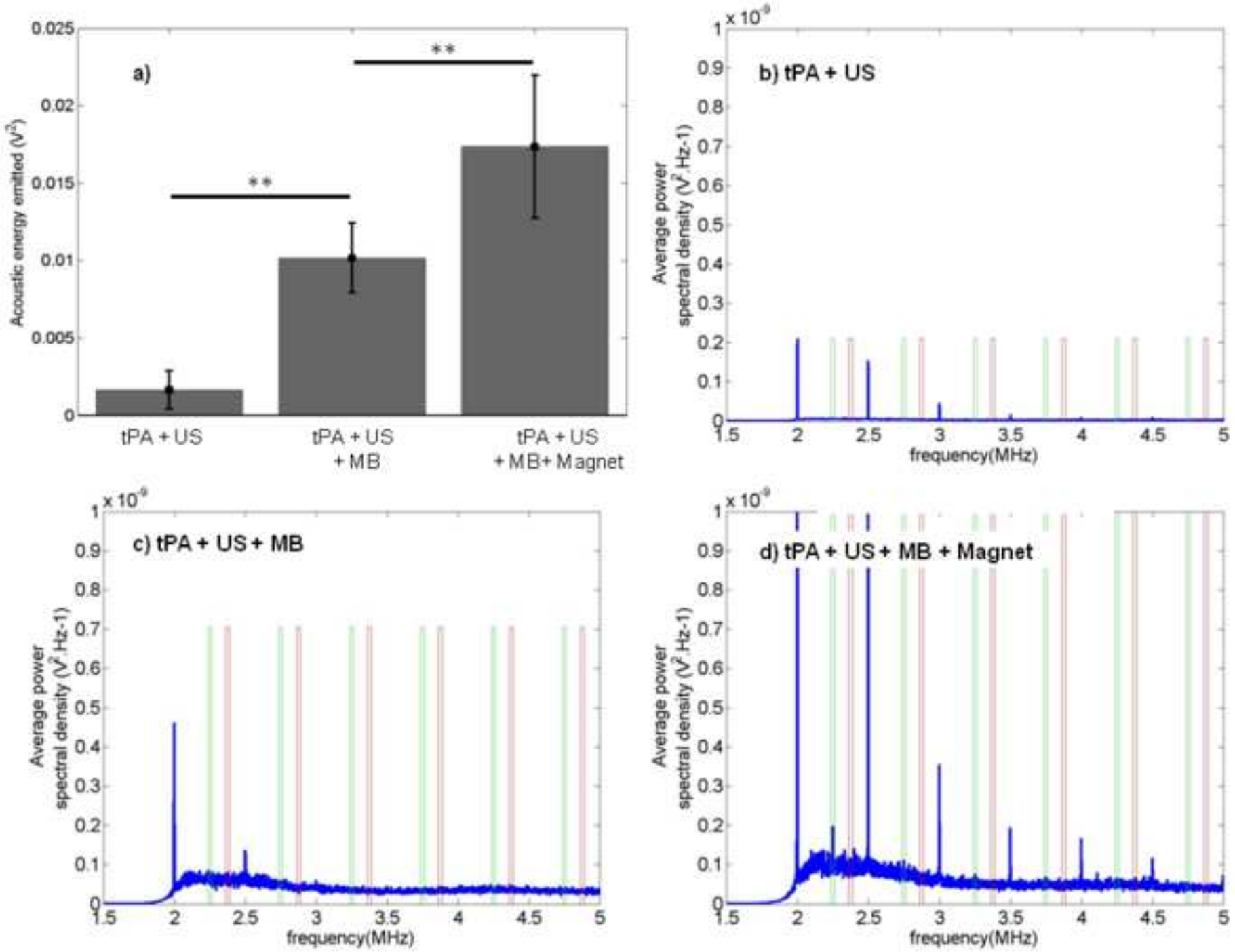

fig8- bivariate.tif
Click here to download high resolution image